

# SNR-Edit: Structure-Aware Noise Rectification for Inversion-Free Flow-Based Editing

Lifan Jiang<sup>1</sup> Boxi Wu<sup>1</sup> Yuhang Pei<sup>1</sup> Tianrun Wu<sup>1</sup> Yongyuan Chen<sup>1</sup> Yan Zhao<sup>2</sup> Shiyu Yu<sup>3</sup> Deng Cai<sup>1</sup>

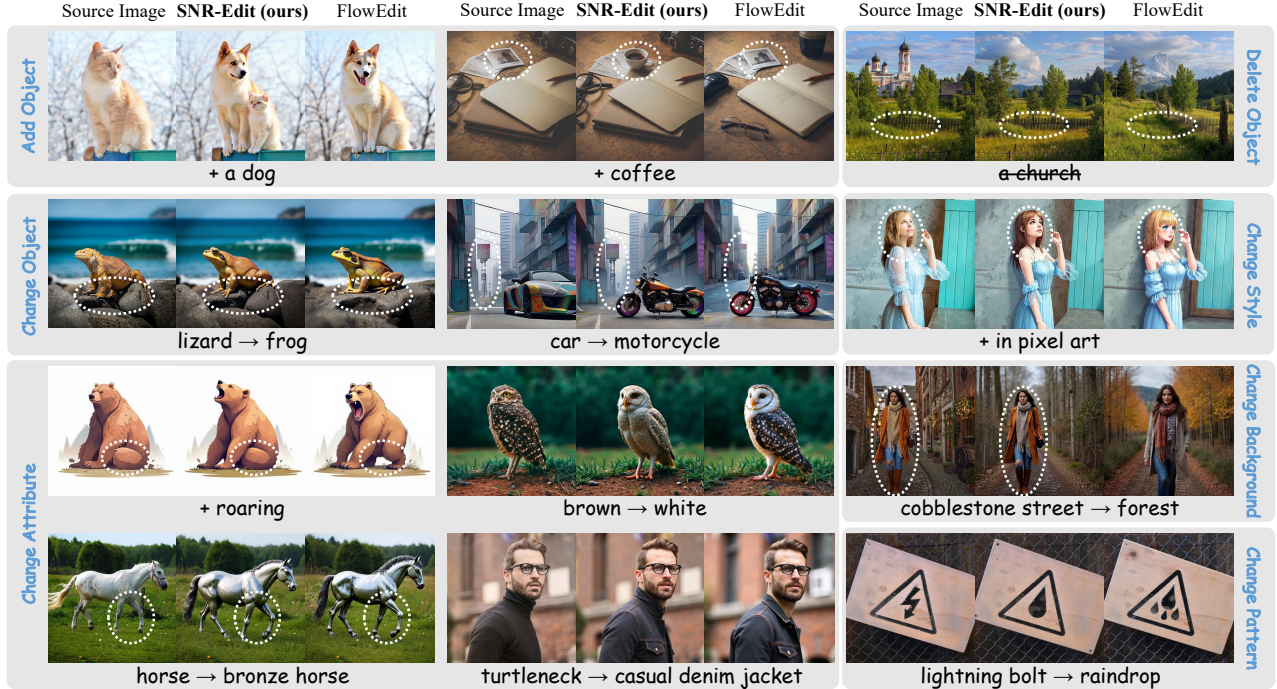


Figure 1: **Qualitative visualization of SNR-Edit results.** Our method demonstrates robust capabilities across a diverse range of tasks, including *Add Object*, *Delete Object*, *Change Object*, *Change Style*, *Change Attribute*, *Change Background*, and *Change Pattern*. Compared to the inversion-free method FlowEdit, SNR-Edit achieves superior structural fidelity, preserving the non-edited layout more faithfully than the baseline while precisely executing the text instructions.

## Abstract

Inversion-free image editing using flow-based generative models challenges the prevailing inversion-based pipelines. However, existing approaches rely on fixed Gaussian noise to construct the source trajectory, leading to biased trajectory dynamics and causing structural degradation or quality loss. To address this, we introduce **SNR-Edit**, a training-free framework

achieving faithful Latent Trajectory Correction via adaptive noise control. Mechanistically, SNR-Edit uses **structure-aware noise rectification** to inject segmentation constraints into the initial noise, anchoring the stochastic component of the source trajectory to the real image’s implicit inversion position and reducing trajectory drift during source–target transport. This lightweight modification yields smoother latent trajectories and ensures high-fidelity structural preservation without requiring model tuning or inversion. Across SD3 and FLUX, evaluations on PIE-Bench and SNR-Bench show that SNR-Edit delivers performance on pixel-level metrics and VLM-based scoring, while adding only  $\sim 1$ s overhead per image.

<sup>1</sup>State Key lab of CAD&CG, Zhejiang University <sup>2</sup>UniTTEC Co. Ltd. <sup>3</sup>Research center, Ningbo Meidong Container Terminal Co.,Ltd.. Correspondence to: Lifan Jiang <lifan-jiang@zju.edu.cn>.

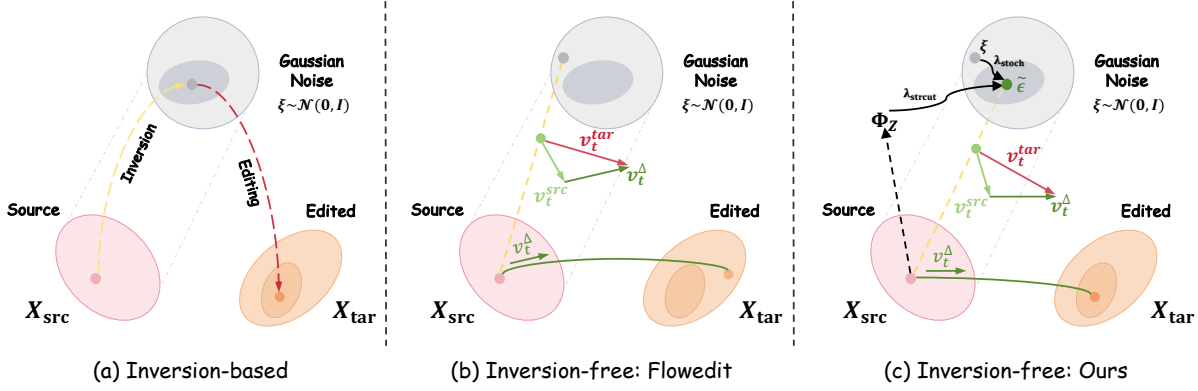


Figure 2: **Schematic comparison of latent editing dynamics.** (a) **Inversion-based methods** rely on a bidirectional mapping to recover latent noise, yet face an inherent fidelity-editability trade-off and high sensitivity to perturbations, making it difficult to maintain structural consistency. (b) **FlowEdit** circumvents inversion but is hindered by a fundamental *Structural–Stochastic Mismatch*. By initiating the flow from content-agnostic Gaussian noise  $\xi \sim \mathcal{N}(0, I)$ , the source proxy is evaluated off the source latent manifold, causing the differential editing trajectory to drift and leading to structural distortion. (c) **Ours**. We introduce structure-aware noise rectification by modulating Gaussian noise with a structural prior  $\Phi_Z$  (prepared by resizing, min–max normalization to  $[-1, 1]$ , and channel-wise broadcasting), forming a rectified noise  $\tilde{\epsilon} = \lambda_{\text{struct}}\Phi_Z + \lambda_{\text{stoch}}\xi$ . This yields a corrected latent source state  $\tilde{Z}_t^{\text{src}} = (1 - t)Z_{\text{src}} + t\tilde{\epsilon}$ , which anchors flow integration and enables a rectified velocity evaluation that preserves structural fidelity while reflecting target semantics.

## 1. Introduction

With the rapid advancement of flow-based generative models (Lipman et al., 2022; Liu et al., 2022), such as SD3 (Esser et al., 2024) and FLUX (Labs et al., 2025), text-guided image editing has advanced toward higher fidelity. The goal is to modify specific semantic attributes of a real image based on textual instructions while preserving the original structural layout and non-edited content.

To achieve this goal, existing works have primarily explored distinct technical routes, yet each faces significant limitations in balancing controllability, efficiency, and fidelity. First, *Inversion-Based Editing* adopts an “invert-and-generate” paradigm to map images back to initial noise (Hertz et al., 2022; Rout et al., 2024; Wang et al., 2024). However, due to the ill-posed nature of inversion, these methods are sensitive to perturbations and suffer from a trade-off between reconstruction fidelity and editability. Second, methods that integrate *Explicit Structural Conditions*, represented by frameworks such as Control-Net (Zhang et al., 2023), offer precise control but incur expensive training overhead and require extensive supervision signals, hindering scalability. Third, *Architectural Feature Injection* (Tumanyan et al., 2023) preserves structure without training. However, the deep coupling with specific network architectures makes these strategies difficult to transfer across evolving foundation models. Finally, recent approaches leveraging *MLLMs* (Brooks et al., 2023; Deng et al., 2025) have improved instruction understanding. Yet, they often lack fine-grained spatial perception, resulting

in structural inconsistencies such as background drift that fail to meet high-fidelity requirements.

Recently, Inversion-Free Editing has emerged as an alternative. Methods like FlowEdit (Kulikov et al., 2025) construct a mapping path by coupling source and target ODE trajectories without unstable inversion. Despite these advances, a critical limitation persists: existing frameworks rely on a proxy Gaussian assumption. We identify that this ignores the mapping relationship between the real image’s distribution and the standard normal prior, creating a *Structural–Stochastic Mismatch* (i.e., source–noise misalignment) and evaluating velocities off the source latent manifold. In high-dimensional latent spaces, this misalignment induces biased trajectory dynamics and inaccurate velocity fields. Consequently, it amplifies trajectory drift during transport, leading to structural degradation in non-edited regions.

To address this, we propose **SNR-Edit**, a training-free framework achieving faithful **Latent Trajectory Correction** via segmentation-guided noise control. Instead of adopting passive fixed-noise initialization, SNR-Edit performs structure-aware noise rectification by injecting segmentation constraints into the initial noise. This anchors the stochastic component of the source trajectory to the source latent neighborhood, reducing drift and yielding smoother transport paths. As a lightweight plug-in, SNR-Edit retains the efficiency of flow-based editing while substantially improving layout stability and fine-grained fidelity (see Figure 1).

Our contributions can be summarized as follows:

1. We reveal the high-dimensional limitations of the fixed-

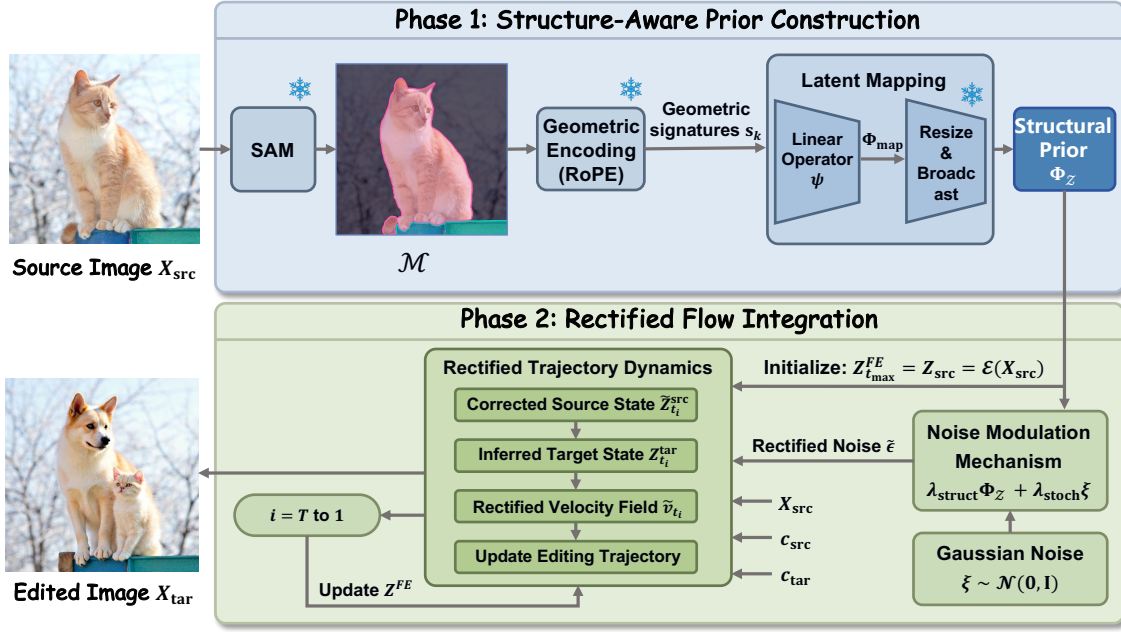


Figure 3: **SNR-Edit Pipeline (cf. Alg. 1).** **Phase 1** (Top) constructs a structural prior by extracting semantic masks  $\mathcal{M}$ , computing geometric signatures  $s_k$ , and forming a single-channel structural map  $\Phi_{\text{map}}$  via a fixed randomized projection  $\psi$ . This map is then resized to the latent resolution, normalized to  $[-1, 1]$ , and broadcast across latent channels to obtain  $\Phi_{\mathcal{Z}}$ . **Phase 2** (Bottom) executes rectified flow integration in latent space. Starting from  $Z_{t_{\max}}^{\text{FE}} = Z_{\text{src}} = \mathcal{E}(X_{\text{src}})$ , the dynamics iteratively update  $Z^{\text{FE}}$  using a rectified velocity field driven by  $\tilde{\epsilon} = \lambda_{\text{struct}}\Phi_{\mathcal{Z}} + \lambda_{\text{stoch}}\xi$ , which mixes  $\Phi_{\mathcal{Z}}$  and Gaussian noise  $\xi$ . This mechanism encourages the output  $X_{\text{tar}} = \mathcal{D}(Z_0^{\text{FE}})$  to preserve the source layout while realizing the target semantics.

noise assumption in existing inversion-free methods, identifying *source-noise misalignment* as the fundamental cause of biased trajectory dynamics and structural degradation, and provide experimental evidence to support these findings.

2. We propose SNR-Edit, a model-agnostic framework that performs **structure-aware noise rectification** via segmentation-guided adaptive noise control, enabling precise latent trajectory correction without requiring model training or inversion.
3. We conduct extensive experiments on SD3 and FLUX over PIE-Bench and SNR-Bench. Evaluated by pixel-level metrics, VLM-based scoring, and a user study, SNR-Edit demonstrates superior performance, significantly surpassing existing methods in terms of structural preservation and overall image quality.

## 2. Related Work

### 2.1. Inversion-Based Edited Approaches

Prevailing image editing methods (Mokady et al., 2023; Rout et al., 2024; Wang et al., 2024; Meng et al., 2021; Parmar et al., 2023) largely rely on the invert-and-generate paradigm within diffusion models to map images back to their starting noise. Despite optimization techniques designed to reduce reconstruction error, these approaches face an inherent trade-off between fidelity and editability. Crucially, even in the ideal scenario of editing synthetic images where the initial noise is fully known, inversion-based baselines still struggle to maintain structural consistency. This indicates that the standard reverse denoising path is highly sensitive to perturbations, making it difficult to preserve the original layout during text-guided editing.

2.2. **Structure-Aware and MLLM-Guided Approaches**

Current research aiming to enhance editing controllability primarily adopts three strategies, yet each faces significant limitations. First, methods (Zhang et al., 2023; Zhao et al., 2023; Mou et al., 2024b;a; Li et al., 2024) that integrate explicit structural conditions achieve precise control but come at the cost of expensive training overhead, requiring task-specific adapters and extensive supervision signals. Second, other approaches rely on complex architectural designs to inject substantial structural information during the sampling phase. This deep coupling with specific network architectures makes these strategies rigid and difficult to transfer across different base models. Finally, while approaches leveraging MLLMs (Deng et al., 2025; Xie et al., 2024; Wu et al., 2025a; Hurst et al., 2024; Li et al., 2025; Wu et al., 2025b; Lin et al., 2025) improve the understanding of complex instructions, they typically lack fine-grained spatial perception. This results in poor structural consistency, rendering them unable to meet the high-fidelity requirements of precise image editing in real-world scenarios.

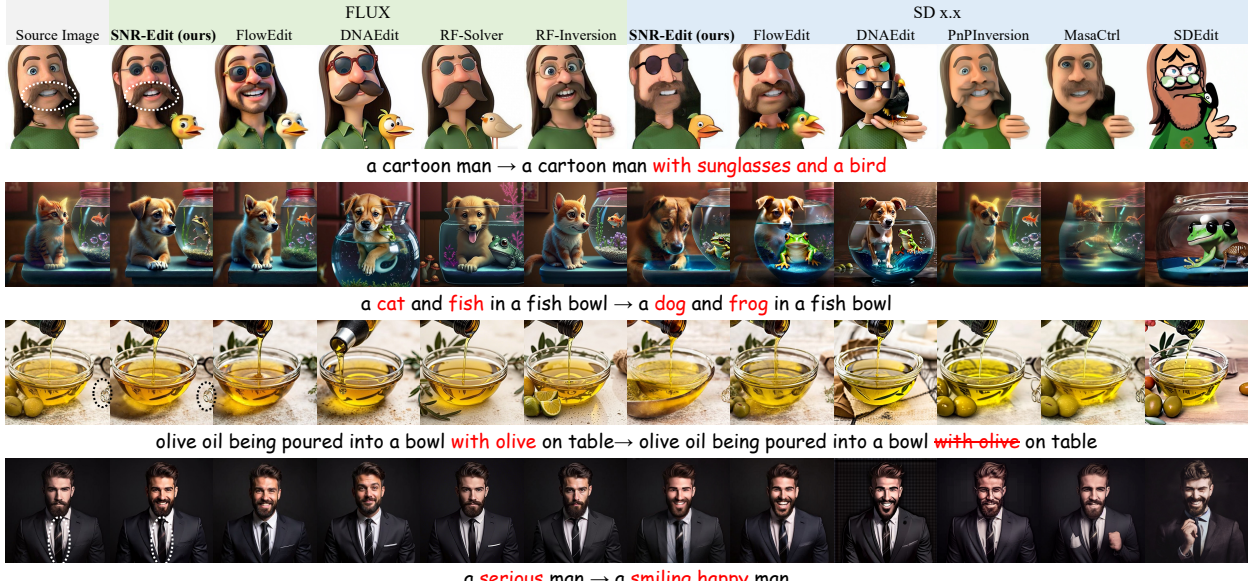


Figure 4: **Visualization of image editing results on PIE-Bench.** Our method demonstrates superior performance across both FLUX and SD backbones, producing images that better preserve structural details, maintain accurate text-image correspondence, and achieve higher overall visual quality compared to existing approaches.

### 2.3. Inversion-Free Flow-Based Editing

Recently, flow-based generative models (Kulikov et al., 2025; Yang et al., 2025; Xie et al., 2025) have enabled efficient inversion-free editing by coupling source and target ODE trajectories, thereby circumventing the unstable inversion process. However, early approaches like FlowEdit (Kulikov et al., 2025) rely on a simplistic, fixed Gaussian noise assumption to approximate the source trajectory, which ignores the geometric discrepancy between the real image manifold and the standard normal prior, leading to a *Structural–Stochastic Mismatch* (i.e., source–noise misalignment) and off-manifold velocity evaluation. Although recent advancements such as DNAEdit (Xie et al., 2025) attempt to mitigate reconstruction error via direct noise alignment or global velocity guidance, they predominantly rest on linear trajectory assumptions and lack explicit region-aware structural constraints. Consequently, a critical source–noise misalignment persists in these frameworks, introducing biased trajectory dynamics that hinder the preservation of complex local structures and precise text-image consistency.

## 3. Methodology

In this section, we present SNR-Edit, a theoretical framework designed to resolve the conflict between stochastic initialization and structural preservation in inversion-free editing. The framework is organized as follows: We first formalize the limitation of existing inversion-free methods as a **Structural–Stochastic Mismatch** in Sec. 3.1. Then, in Sec. 3.2, we introduce the **Structure-Aware Prior Construction** (Figure 3 phase 1), which injects instance-specific geometric constraints via semantic region decom-

position and randomized geometric projection. Finally, in Sec. 3.3, we derive the **Rectified Flow Integration** (Figure 3 phase 2), which anchors the editing dynamics in the latent space through structure-aware noise modulation.

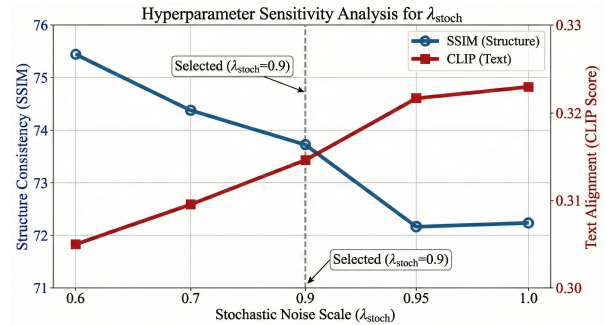


Figure 5: **Sensitivity analysis of the stochastic scale  $\lambda_{\text{stoch}}$ .** We observe a trade-off between structural consistency (SSIM) and text alignment (CLIP), identifying 0.9 as the optimal balance for text-guided image editing.

### 3.1. Preliminaries: Structural–Stochastic Mismatch

Flow Matching models transport a source distribution  $p_0$  to a target distribution  $p_1$  via a time-dependent velocity field  $v(\cdot, t, c)$  conditioned on prompt  $c$ . We operate in the latent space of a pre-trained Autoencoder. Let  $Z_{\text{src}} = \mathcal{E}(X_{\text{src}})$  denote the latent representation of the source image  $X_{\text{src}}$ . In inversion-free editing, the edited trajectory  $Z_t^{\text{FE}}$  is commonly formulated using a difference-of-flows dynamic:

$$\dot{Z}_t^{\text{FE}} = v(Z_t^{\text{FE}}, t, c_{\text{tar}}) - v(Z_t^{\text{src}}, t, c_{\text{src}}), \quad (1)$$



Figure 6: **Visualization of image editing results on SNR-Bench.** In the above examples, our method demonstrates superior performance on both FLUX and SD architectures, surpassing existing baselines in terms of maintaining structural integrity, aligning with text prompts, and generating high-quality visuals across a diverse set of challenging inputs.

where  $Z_t^{\text{src}}$  denotes a proxy of the source latent trajectory.

Existing inversion-free methods typically approximate the source trajectory by a fixed Gaussian interpolation:

$$Z_t^{\text{src}} \approx (1-t)Z_{\text{src}} + t\xi, \quad \xi \sim \mathcal{N}(\mathbf{0}, \mathbf{I}), \quad (2)$$

which avoids costly inversion but introduces a fundamental limitation (see Figure 2(b)).

**Structural-Stochastic Mismatch.** Since the Gaussian noise  $\xi$  is content-agnostic, the proxy  $Z_t^{\text{src}}$  deviates from the local geometric manifold of  $Z_{\text{src}}$ . As a result, the velocity field  $v(\cdot)$  is evaluated off-manifold during integration, leading to trajectory drift and structural degradation (e.g., background distortion) in the edited result.

### 3.2. Structure-Aware Prior Construction

To mitigate this mismatch, we propose Figure 3 phase 1 of our framework: injecting instance-specific geometric constraints into the stochastic initialization.

**Semantic Region Decomposition via SAM2.** Given the pixel-space source image  $X_{\text{src}} \in \mathbb{R}^{H \times W \times 3}$ , we leverage **SAM2** (Ravi et al., 2024) (specifically the Hiera-Large variant) to explicitly extract instance-level semantic regions. To ensure robustness, we apply a stability filter (discarding scores  $< 0.85$ ) together with simple area-based screening to obtain a filtered set of stable masks  $\mathcal{M} = \{m_1, \dots, m_K\}$ . This mask-based decomposition facilitates reliable boundary delineation in practice, thereby reducing cross-region feature leakage during subsequent processing.

**Geometric Encoding with RoPE.** To capture the spatial layout, we encode pixel coordinates via RoPE into a  $C$ -dimensional embedding. Unlike absolute encodings, RoPE

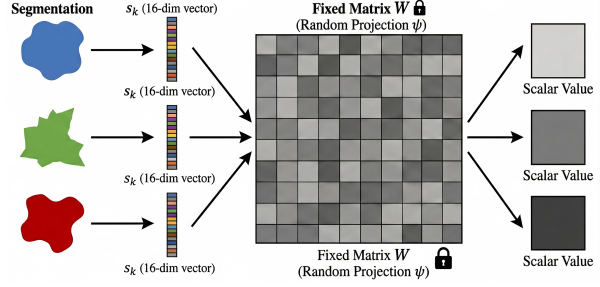


Figure 7: **Illustration of the Randomized Geometric Projection.** The fixed projection  $\psi$ , initialized with frozen random weights, maps high-dimensional geometric signatures ( $s_k$ ) to distinct scalar intensities. This acts as a structural hash, assigning unique identifiers to spatial regions without requiring training or additional supervision.

naturally incorporates relative spatial information, allowing the aggregated descriptor to robustly represent the internal geometric configuration of irregular masks. For each region  $m_k$ , a regional geometric descriptor is computed as:

$$\mathbf{s}_k = \frac{1}{|m_k|} \sum_{\mathbf{p} \in m_k} \text{RoPE}(\mathbf{p}), \quad (3)$$

where  $\mathbf{p}$  denotes normalized pixel coordinates. This descriptor summarizes region-level spatial information, such as the centroid and spatial extent.

**Randomized Geometric Projection.** To map the high-dimensional geometric signatures into a latent structural constraint, we employ a randomized projection strategy (Figure 7). Each regional descriptor  $\mathbf{s}_k \in \mathbb{R}^C$  is mapped to

a scalar intensity via a fixed projection  $\psi : \mathbb{R}^C \rightarrow \mathbb{R}$ . Formally,  $\psi$  is a linear projection  $\psi : \mathbb{R}^C \rightarrow \mathbb{R}$  parameterized by a weight vector  $W \in \mathbb{R}^{1 \times C}$  (i.e., a  $1 \times C$  row matrix).

To ensure unbiased geometric hashing,  $W$  is initialized from a uniform distribution  $\mathcal{U}(-\frac{1}{\sqrt{C}}, \frac{1}{\sqrt{C}})$  and remains frozen (non-trainable) throughout the inference process.

Inspired by the classic concept of random projections (Johnson et al., 1984),  $\psi$  acts as a randomized geometric hash. While strict isometry typically requires higher embedding dimensions, the resulting 1D projection provides region-specific intensity signatures that empirically exhibit low collision under our mask filtering regime. The resulting structural map is formulated as: *Overlaps are resolved by highest-stability assignment.*

$$\Phi_{\text{map}}(\mathbf{p}) = \sum_{k=1}^K \psi(\mathbf{s}_k) \mathbb{I}_{m_k}(\mathbf{p}). \quad (4)$$

Since the weights are fixed,  $\psi$  serves as a deterministic structural anchor. Finally, we resize  $\Phi_{\text{map}}$  to the latent resolution, normalize it to  $[-1, 1]$  via min–max scaling (with a zero-map fallback when the range is negligible), and broadcast it across latent channels to obtain the latent structural prior  $\Phi_{\mathcal{Z}}$ , matching the shape of the latent noise.

#### Algorithm 1 Inversion-Free Editing via SNR-Edit

```

1: Input: Source Image  $X_{\text{src}}$ , Prompts  $c_{\text{src}}, c_{\text{tar}}$ , Steps
    $\{t_i\}_{i=0}^T$ , Scales  $\lambda_{\text{struct}}, \lambda_{\text{stoch}}$ 
2: Output: Edited image  $X_{\text{tar}}$ 
3: Init: Encode source  $Z_{\text{src}} \leftarrow \mathcal{E}(X_{\text{src}})$ 
4: Init:  $Z_{t_{\max}}^{\text{FE}} \leftarrow Z_{\text{src}}$  {Initialize trajectory}
5: // PHASE 1: STRUCTURE-AWARE PRIOR CONSTRUCTION
6:  $\mathcal{M} \leftarrow \text{Segment}(X_{\text{src}})$  {SAM2 on pixel space}
7:  $\Phi_{\mathcal{Z}} \leftarrow \text{ComputePrior}(\mathcal{M}, \text{RoPE})$  {Obtain latent prior
   via Equation (4)}
8: // PHASE 2: RECTIFIED FLOW INTEGRATION
9: for  $i = T$  to 1 do
10:    $\xi \sim \mathcal{N}(\mathbf{0}, \mathbf{I})$ 
11:    $\tilde{\epsilon} \leftarrow \lambda_{\text{struct}} \Phi_{\mathcal{Z}} + \lambda_{\text{stoch}} \xi$  {Noise Modulation}
12:    $\tilde{Z}_{t_i}^{\text{src}} \leftarrow (1 - t_i) Z_{\text{src}} + t_i \tilde{\epsilon}$  {Corrected latent source
   state}
13:   // CALCULATE STRUCTURAL OFFSET
14:    $\Delta \tilde{Z}_{t_i} \leftarrow \tilde{Z}_{t_i}^{\text{src}} - Z_{\text{src}}$  {Dynamic geometric anchor}
15:   // RECTIFIED VELOCITY EVALUATION
16:    $\tilde{v}_{t_i} \leftarrow v(Z_{t_i}^{\text{FE}} + \Delta \tilde{Z}_{t_i}, t_i, c_{\text{tar}}) - v(\tilde{Z}_{t_i}^{\text{src}}, t_i, c_{\text{src}})$ 
17:    $Z_{t_{i-1}}^{\text{FE}} \leftarrow Z_{t_i}^{\text{FE}} + (t_{i-1} - t_i) \tilde{v}_{t_i}$  {Update latent trajectory}
18: end for
19: Return:  $X_{\text{tar}} = \mathcal{D}(Z_0^{\text{FE}})$  {Decode to pixel space}

```

### 3.3. Rectified Flow Integration

In Figure 3 phase 2, we perform editing by rectifying the stochastic initialization used in the inversion-free dynamics.

**Structure-Aware Noise Rectification.** During prior preparation, we resize  $\Phi_{\mathcal{Z}}$  to the latent resolution and normalize it to the bounded range  $[-1, 1]$  via min–max scaling (with a zero-map fallback when the value range is negligible). This bounded preprocessing keeps the structural signal at a stable magnitude comparable to latent noise used by the pre-trained model, thereby mitigating out-of-distribution behavior (see analysis in Section B). We then construct a rectified noise by combining this normalized prior with Gaussian noise (see Figure 2(c); analysis in Figure 5):

$$\tilde{\epsilon} = \lambda_{\text{struct}} \Phi_{\mathcal{Z}} + \lambda_{\text{stoch}} \xi, \quad \xi \sim \mathcal{N}(\mathbf{0}, \mathbf{I}). \quad (5)$$

Using this rectified noise  $\tilde{\epsilon}$ , we compute the corrected source state  $\tilde{Z}_t^{\text{src}}$  following the update rule in Alg. 1, which serves as a stable geometric anchor for subsequent flow integration.

**Rectified Editing Dynamics.** To ensure strict structural alignment, we introduce a rectified flow dynamic that compensates for geometric deviations. Specifically, we evaluate the target velocity not at the drifting current state, but at a corrected position “re-anchored” to the source manifold. This forces the generative flow to respect the original layout constraints while evolving semantic content. We reformulate the editing ODE as: *Implementation:* We discretize Eq. (6) over  $\{t_i\}$  and re-sample  $\xi$  each step (Alg. 1).

$$\tilde{Z}_t^{\text{FE}} = v(Z_t^{\text{FE}} + \Delta \tilde{Z}_t, t, c_{\text{tar}}) - v(\tilde{Z}_t^{\text{src}}, t, c_{\text{src}}), \quad (6)$$

where  $\Delta \tilde{Z}_t$  represents the time-dependent structural offset in the latent space, defined as:

$$\Delta \tilde{Z}_t = \tilde{Z}_t^{\text{src}} - Z_{\text{src}}. \quad (7)$$

By explicitly incorporating this offset into the target velocity evaluation, SNR-Edit anchors the editing trajectory to the corrected geometric manifold, thereby preserving layout consistency while enabling precise semantic manipulation. A Lipschitz stability analysis further shows that the re-anchored evaluation in Eq. (6) yields a controlled vector-field error and a bounded trajectory deviation (Section B.3, Eq. (16)–(18)).

## 4. Experiments

### 4.1. Experimental Settings

**Datasets and Benchmarks.** We evaluate on two benchmarks to cover varying complexities. First, we use **PIE-Bench** (Ju et al., 2023) (700 images) for standard quantitative evaluation. Second, to address the lack of high-resolution and semantically diverse samples in existing sets, we construct **SNR-Bench** (see Section A). It comprises 80 high-quality images:  $\sim 50\%$  sampled from PIE-Bench for

Table 1: **Quantitative comparison on PIE-Bench.** We evaluate methods across SD 1.x, SD3, and FLUX backbones. Methods are categorized by their mechanism: **Inv-B** (Inversion-Based), **Inv-F** (Inversion-Free). **Bold** indicates the best result, and underline indicates the second best across all methods (global comparison). The **Avg. Rank** is calculated across all methods (global ranking). Our **SNR-Edit** demonstrates superior performance across all evaluated metrics.

Backbone	Method	Type	Dist ( $\times 10^3$ ) $\downarrow$	PSNR $\uparrow$	LPIPS ( $\times 10^3$ ) $\downarrow$	MSE ( $\times 10^4$ ) $\downarrow$	SSIM ( $\times 10^2$ ) $\uparrow$	CLIP $\uparrow$	Avg. Rank $\downarrow$
SD 1.x	SDEdit (SD1.5)	Inv-B	197.01	14.43	538.76	2754.35	43.41	0.314	9.83
	MasaCtrl (SD1.4)	Inv-B	119.37	18.85	267.56	1011.02	68.98	0.293	5.83
	PnPInversion (SD1.4)	Inv-B	<u>93.93</u>	<u>20.93</u>	211.94	<u>627.28</u>	73.13	0.304	3.33
SD3	DNAEdit	Inv-F	164.61	15.96	452.57	1871.58	58.82	<u>0.318</u>	8.50
	FlowEdit	Inv-F	128.69	18.17	300.39	1162.54	72.23	<u>0.323</u>	5.67
<b>SNR-Edit (Ours)</b>		Inv-F	121.85	18.62	279.12	1037.96	<u>73.74</u>	0.315	4.50
FLUX	RF-Inversion	Inv-B	113.69	19.36	342.16	929.17	57.61	0.288	6.67
	RF-Solver	Inv-B	108.80	19.77	352.47	853.59	70.62	0.305	5.00
	DNAEdit	Inv-F	158.02	16.38	435.90	1742.18	61.90	0.313	8.17
	FlowEdit	Inv-F	129.82	18.19	299.42	1199.97	73.33	0.307	6.17
	<b>SNR-Edit (Ours)</b>	Inv-F	<b>91.35</b>	<b>21.32</b>	<b>195.36</b>	<b>607.07</b>	<b>79.96</b>	0.294	<b>2.33</b>

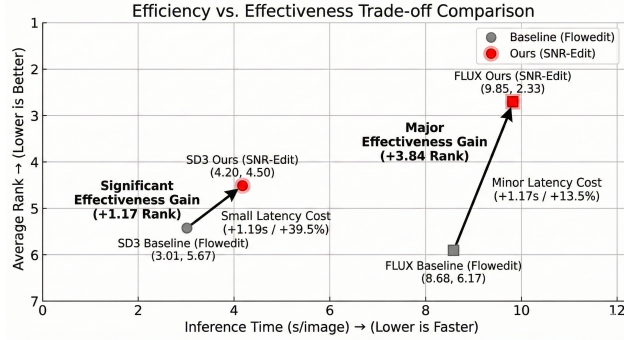


Figure 8: **Efficiency vs. Effectiveness Trade-off on PIE-Bench.** The comparisons are conducted on a single A100 GPU. The axes contrast inference latency against the Average Rank (sourced from Table 1). Compared to FlowEdit, SNR-Edit achieves significant performance gains with only a marginal increase in latency. This indicates that our method offers a highly favorable trade-off, significantly enhancing generation quality at an acceptable speed cost on both SD3 and FLUX architectures.

continuity and  $\sim 50\%$  web-collected for rich textural details. We cover four editing operations: *adjust*, *change*, *remove*, and *add*. Prompts for non-PIE images are manually verified to ensure clarity and minimize ambiguity.

**Baselines and Implementation.** We implement **SNR-Edit** on SD3 (Esser et al., 2024) and FLUX (Labs et al., 2025). We compare against inversion-based (RF-Inversion (Rout et al., 2024), RF-Solver (Wang et al., 2024), SDEdit (Meng et al., 2021), PnPInversion (Tumanyan et al., 2023), MasaCtrl (Cao et al., 2023), FTEdit (Xu et al., 2025)) and inversion-free approaches (DNAEdit (Xie et al., 2025), FlowEdit (Kulikov et al., 2025)). For fair comparison, all inversion-free baselines use unified sampling configurations on the same base model, while others follow their original settings.

**Ablation Variants.** To validate each component’s effectiveness, we evaluate three variants on the SD3 backbone: (1)

w/o *Semantic Decomp.* removes Semantic Region Decomposition, applying RoPE and projection to the global image; (2) w/o *RoPE* discards geometric embeddings, relying solely on binary masks from SAM; (3) w/o *Rand. Proj.* replaces the randomized linear projection with average pooling.

**Evaluation Metrics.** We assess structural consistency, background preservation, and semantic alignment using three protocols: (1) *Quantitative Metrics*: On PIE-Bench, we report latent distance (structure), PSNR/SSIM/MSE/LPIPS (background/perceptual), and CLIP similarity (alignment). (2) *VLM Evaluation*: On SNR-Bench, we employ ImgEdit Reward (Ye et al., 2025) and Qwen-VL 32B (Bai et al., 2025) to score Structural Fidelity, Text-Image Alignment, and Background Consistency, capturing global coherence often missed by low-level metrics (details in Section C). (3) *User Study*: We conducted a randomized blind user study with 38 valid participants (from 40 recruited). Each completed 20 randomized comparison tasks under a strictly anonymous protocol provided in Section D.

## 4.2. Main Results

**Visualization of image editing results.** Figures 4 and 6 highlight SNR-Edit’s superiority across FLUX and SD3 backbones on both PIE-Bench and SNR-Bench. Our method demonstrates precise semantic manipulation, seamlessly integrating requested elements while strictly preserving subject identity, geometric consistency, and high-frequency details (e.g., tattoos). This significantly outperforms baselines that often suffer from severe identity drift, distortion, or over-smoothing. Furthermore, the efficiency analysis in Figure 8 confirms that SNR-Edit achieves these substantial qualitative gains with negligible latency overhead compared to FlowEdit, demonstrating an optimal balance between high-fidelity editing and practical deployment efficiency.

**Quantitative Analysis on Pixel-Level Metrics.** As shown in Table 1, SNR-Edit establishes a new SOTA among inversion-free baselines on PIE-Bench. With the

Table 2: **Perceptual Evaluation via VLMs and User Study.** We report assessment results (1–5) using advanced reward models (ImgEdit Reward & Qwen-VL) and a human user study. Methods are grouped by backbone: SD x.x, SD3, and FLUX. **Bold** indicates the best result, and underline indicates the second best across all methods (global comparison). The **Avg. Rank** is calculated across all methods (global ranking), demonstrating that SNR-Edit outperforms all baselines.

Backbone	Method	ImgEdit Reward Model			Qwen-VL32B			User Study			Avg. Rank ↓
		Struct ↑	Text ↑	BG ↑	Struct ↑	Text ↑	BG ↑	Struct ↑	Text ↑	Qual ↑	
SD x.x	SDEdit (SD1.5)	2.53	2.49	2.69	1.63	2.51	1.31	2.15	2.85	2.40	11.33
	MasaCtrl (SD1.4)	3.04	2.46	3.31	2.49	1.95	2.59	2.65	2.15	2.55	9.56
	PnPInversion (SD1.4)	3.48	3.03	3.80	3.58	2.84	2.94	3.60	2.95	3.25	5.67
	FTEdit (SD3.5)	<b>3.55</b>	<u>3.30</u>	3.99	3.58	3.23	3.25	3.70	3.40	3.75	2.89
SD3	DNAEdit	2.75	2.70	2.98	2.30	3.21	1.80	2.60	3.35	2.95	8.67
	FlowEdit	3.34	3.19	3.90	3.35	<b>3.65</b>	3.28	3.45	<b>3.80</b>	3.50	4.11
	<b>SNR-Edit (Ours)</b>	3.44	<u>3.30</u>	4.08	3.40	3.58	<u>3.30</u>	3.65	<u>3.75</u>	3.85	2.56
FLUX	RF-Inversion	3.36	2.94	3.70	2.99	2.63	2.31	3.20	2.90	3.10	7.67
	RF-Solver	2.42	2.40	2.47	2.41	3.19	1.89	2.55	3.10	2.65	10.00
	DNAEdit	2.86	2.85	3.16	2.03	3.20	1.75	2.90	3.15	2.80	8.67
	FlowEdit	3.38	3.21	4.04	3.28	3.39	3.19	3.50	3.55	3.45	4.33
	<b>SNR-Edit (Ours)</b>	<b>3.55</b>	<b>3.38</b>	<b>4.24</b>	<b>3.80</b>	3.09	<b>3.80</b>	<b>3.90</b>	3.40	<b>3.95</b>	<b>2.11</b>

Table 3: **Ablation Study.** We analyze the contribution of each module in the structure-aware prior construction phase using the SD3 backbone. The “Baseline” represents the method without any proposed components (equivalent to FlowEdit). Text-Image alignment scores are evaluated by Qwen3VL-32B to measure semantic alignment.

Method Variant	Dist ( $\times 10^3$ ) ↓	SSIM ( $\times 10^2$ ) ↑	LPIPS ( $\times 10^3$ ) ↓	Text ↑
Baseline (FlowEdit)	128.69	72.23	300.39	3.386
w/o Semantic Decomp.	130.47	71.93	303.63	3.309
w/o RoPE (Binary Masks)	129.12	72.67	290.21	3.210
w/o Rand. Proj. (Avg Pooling)	128.82	72.58	291.27	3.251
<b>SNR-Edit (Ours)</b>	<b>121.85</b>	<b>73.74</b>	<b>279.12</b>	<b>3.568</b>

FLUX backbone, it achieves the lowest Structural Distance (91.35) and LPIPS (195.36), outperforming RF-Solver and FlowEdit. Our method also surpasses FlowEdit in average ranking (2.33 vs. 6.17), demonstrating a strong balance between structural preservation and semantic alignment. These results validate that our geometric noise rectification effectively mitigates structural degradation.

**Perceptual Evaluation with VLM Reward Models.** Table 2 confirms SNR-Edit’s dominance on SNR-Bench using VLMs (ImgEdit Reward (Ye et al., 2025) and Qwen-VL 32B). With FLUX, our method achieves the best average rank (2.11), surpassing all optimization-based methods in this benchmark. Similarly, in the SD3 group, SNR-Edit achieves the best average rank (2.56), exceeding FlowEdit in both alignment and preservation metrics. Evaluation details are provided in Section C.

**User Study Validation.** We conducted a blinded user study with 38 participants (protocol in Section D). Results in Table 2 corroborate the VLM evaluations, with SNR-Edit achieving the highest satisfaction scores in both SD3 and FLUX groups (Quality 3.85 and 3.95). Notably, our FLUX-based method yields the highest global score (3.95), sur-

passing even optimization-based FTEdit (Xu et al., 2025) (3.75), highlighting its efficacy in generating photorealistic and structurally coherent edits.

### 4.3. Ablation Study

Table 3 quantifies the impact of each module on the SD3 backbone. Semantic Decomposition emerges as the most influential factor; omitting it maximizes distortion (Dist hits 130.47), verifying the need for regional priors. RoPE is crucial for spatial alignment, as substituting it with binary masks lowers SSIM to 72.67. Furthermore, Randomized Projection preserves geometric details better than average pooling. Ultimately, the complete SNR-Edit framework achieves an optimal balance between structural fidelity (121.85 Dist) and text-image alignment.

## 5. Conclusion

We identify the Structural–Stochastic Mismatch induced by the fixed Gaussian proxy in inversion-free editing as a key bottleneck, which biases transport dynamics and leads to structural drift. To address this, we propose **SNR-Edit**, a training-free and model-agnostic framework that anchors inversion-free editing with an instance-specific geometric prior. Our method constructs a spatially-guided latent prior via semantic region decomposition and spatial encoding, and then rectifies stochastic initialization through fixed-ratio noise modulation. By replacing the biased source proxy with a structure-aware trajectory anchor, SNR-Edit stabilizes the editing dynamics and improves structural consistency without the computational overhead of inversion or fine-tuning. Extensive experiments on SD3 and FLUX, with VLM-based evaluation and a user study, demonstrate significant gains in structural preservation, semantic alignment, and perceptual quality. These results highlight the importance of trajectory engineering via structure-aware initialization for robust and controllable flow-based image editing.

## References

Bai, S., Cai, Y., Chen, R., Chen, K., Chen, X., Cheng, Z., Deng, L., Ding, W., Gao, C., Ge, C., Ge, W., Guo, Z., Huang, Q., Huang, J., Huang, F., Hui, B., Jiang, S., Li, Z., Li, M., Li, M., Li, K., Lin, Z., Lin, J., Liu, X., Liu, J., Liu, C., Liu, Y., Liu, D., Liu, S., Lu, D., Luo, R., Lv, C., Men, R., Meng, L., Ren, X., Ren, X., Song, S., Sun, Y., Tang, J., Tu, J., Wan, J., Wang, P., Wang, P., Wang, Q., Wang, Y., Xie, T., Xu, Y., Xu, H., Xu, J., Yang, Z., Yang, M., Yang, J., Yang, A., Yu, B., Zhang, F., Zhang, H., Zhang, X., Zheng, B., Zhong, H., Zhou, J., Zhou, F., Zhou, J., Zhu, Y., and Zhu, K. Qwen3-vl technical report, 2025. URL <https://arxiv.org/abs/2511.21631>.

Brooks, T., Holynski, A., and Efros, A. A. Instructpix2pix: Learning to follow image editing instructions. In *Proceedings of the IEEE/CVF conference on computer vision and pattern recognition*, pp. 18392–18402, 2023.

Cao, M., Wang, X., Qi, Z., Shan, Y., Qie, X., and Zheng, Y. Masactrl: Tuning-free mutual self-attention control for consistent image synthesis and editing. In *Proceedings of the IEEE/CVF international conference on computer vision*, pp. 22560–22570, 2023.

Deng, C., Zhu, D., Li, K., Gou, C., Li, F., Wang, Z., Zhong, S., Yu, W., Nie, X., Song, Z., Shi, G., and Fan, H. Emerging properties in unified multimodal pretraining, 2025. URL <https://arxiv.org/abs/2505.14683>.

Esser, P., Kulal, S., Blattmann, A., Entezari, R., Müller, J., Saini, H., Levi, Y., Lorenz, D., Sauer, A., Boesel, F., Podell, D., Dockhorn, T., English, Z., Lacey, K., Goodwin, A., Marek, Y., and Rombach, R. Scaling rectified flow transformers for high-resolution image synthesis, 2024. URL <https://arxiv.org/abs/2403.03206>.

Hertz, A., Mokady, R., Tenenbaum, J., Aberman, K., Pritch, Y., and Cohen-Or, D. Prompt-to-prompt image editing with cross attention control. *arXiv preprint arXiv:2208.01626*, 2022.

Hurst, A., Lerer, A., Goucher, A. P., Perelman, A., Ramesh, A., Clark, A., Ostrow, A., Welihinda, A., Hayes, A., Radford, A., et al. Gpt-4o system card. *arXiv preprint arXiv:2410.21276*, 2024.

Johnson, W. B., Lindenstrauss, J., et al. Extensions of lipschitz mappings into a hilbert space. *Contemporary mathematics*, 26(189-206):1, 1984.

Ju, X., Zeng, A., Bian, Y., Liu, S., and Xu, Q. Direct inversion: Boosting diffusion-based editing with 3 lines of code. *arXiv preprint arXiv:2310.01506*, 2023.

Kulikov, V., Kleiner, M., Huberman-Spiegelglas, I., and Michaeli, T. Flowedit: Inversion-free text-based editing using pre-trained flow models. In *Proceedings of the IEEE/CVF International Conference on Computer Vision*, pp. 19721–19730, 2025.

Labs, B. F., Batifol, S., Blattmann, A., Boesel, F., Consul, S., Diagne, C., Dockhorn, T., English, J., English, Z., Esser, P., Kulal, S., Lacey, K., Levi, Y., Li, C., Lorenz, D., Müller, J., Podell, D., Rombach, R., Saini, H., Sauer, A., and Smith, L. Flux.1 kontext: Flow matching for in-context image generation and editing in latent space, 2025. URL <https://arxiv.org/abs/2506.15742>.

Li, H., Zhang, M., Zheng, D., Guo, Z., Jia, Y., Feng, K., Yu, H., Liu, Y., Feng, Y., Pei, P., et al. Editthinker: Unlocking iterative reasoning for any image editor. *arXiv preprint arXiv:2512.05965*, 2025.

Li, M., Yang, T., Kuang, H., Wu, J., Wang, Z., Xiao, X., and Chen, C. Controlnet++: Improving conditional controls with efficient consistency feedback: Project page: liming-ai. github. io/controlnet\_plus\_plus. In *European Conference on Computer Vision*, pp. 129–147. Springer, 2024.

Lin, B., Li, Z., Cheng, X., Niu, Y., Ye, Y., He, X., Yuan, S., Yu, W., Wang, S., Ge, Y., et al. Uniworld: High-resolution semantic encoders for unified visual understanding and generation. *arXiv preprint arXiv:2506.03147*, 2025.

Lipman, Y., Chen, R. T., Ben-Hamu, H., Nickel, M., and Le, M. Flow matching for generative modeling. *arXiv preprint arXiv:2210.02747*, 2022.

Liu, X., Gong, C., and Liu, Q. Flow straight and fast: Learning to generate and transfer data with rectified flow. *arXiv preprint arXiv:2209.03003*, 2022.

Meng, C., He, Y., Song, Y., Song, J., Wu, J., Zhu, J.-Y., and Ermon, S. Sdedit: Guided image synthesis and editing with stochastic differential equations. *arXiv preprint arXiv:2108.01073*, 2021.

Mokady, R., Hertz, A., Aberman, K., Pritch, Y., and Cohen-Or, D. Null-text inversion for editing real images using guided diffusion models. In *Proceedings of the IEEE/CVF conference on computer vision and pattern recognition*, pp. 6038–6047, 2023.

Mou, C., Wang, X., Xie, L., Wu, Y., Zhang, J., Qi, Z., and Shan, Y. T2i-adapter: Learning adapters to dig out more controllable ability for text-to-image diffusion models. In *Proceedings of the AAAI conference on artificial intelligence*, volume 38, pp. 4296–4304, 2024a.

Mou, C., Wang, X., Xie, L., Wu, Y., Zhang, J., Qi, Z., and Shan, Y. T2i-adapter: Learning adapters to dig out more controllable ability for text-to-image diffusion models. In *Proceedings of the AAAI conference on artificial intelligence*, volume 38, pp. 4296–4304, 2024b.

Parmar, G., Kumar Singh, K., Zhang, R., Li, Y., Lu, J., and Zhu, J.-Y. Zero-shot image-to-image translation. In *ACM SIGGRAPH 2023 conference proceedings*, pp. 1–11, 2023.

Ravi, N., Gabeur, V., Hu, Y.-T., Hu, R., Ryali, C., Ma, T., Khedr, H., Rädl, R., Rolland, C., Gustafson, L., et al. Sam 2: Segment anything in images and videos. *arXiv preprint arXiv:2408.00714*, 2024.

Rout, L., Chen, Y., Ruiz, N., Caramanis, C., Shakkottai, S., and Chu, W.-S. Semantic image inversion and editing using rectified stochastic differential equations. *arXiv preprint arXiv:2410.10792*, 2024.

Tumanyan, N., Geyer, M., Bagon, S., and Dekel, T. Plug-and-play diffusion features for text-driven image-to-image translation. In *Proceedings of the IEEE/CVF conference on computer vision and pattern recognition*, pp. 1921–1930, 2023.

Wang, J., Pu, J., Qi, Z., Guo, J., Ma, Y., Huang, N., Chen, Y., Li, X., and Shan, Y. Taming rectified flow for inversion and editing. *arXiv preprint arXiv:2411.04746*, 2024.

Wu, C., Li, J., Zhou, J., Lin, J., Gao, K., Yan, K., ming Yin, S., Bai, S., Xu, X., Chen, Y., Chen, Y., Tang, Z., Zhang, Z., Wang, Z., Yang, A., Yu, B., Cheng, C., Liu, D., Li, D., Zhang, H., Meng, H., Wei, H., Ni, J., Chen, K., Cao, K., Peng, L., Qu, L., Wu, M., Wang, P., Yu, S., Wen, T., Feng, W., Xu, X., Wang, Y., Zhang, Y., Zhu, Y., Wu, Y., Cai, Y., and Liu, Z. Qwen-image technical report, 2025a. URL <https://arxiv.org/abs/2508.02324>.

Wu, C., Zheng, P., Yan, R., Xiao, S., Luo, X., Wang, Y., Li, W., Jiang, X., Liu, Y., Zhou, J., et al. Omnipgen2: Exploration to advanced multimodal generation. *arXiv preprint arXiv:2506.18871*, 2025b.

Xie, C., Li, M., Li, S., Wu, Y., Yi, Q., and Zhang, L. Dnaedit: Direct noise alignment for text-guided rectified flow editing. *arXiv preprint arXiv:2506.01430*, 2025.

Xie, J., Mao, W., Bai, Z., Zhang, D. J., Wang, W., Lin, K. Q., Gu, Y., Chen, Z., Yang, Z., and Shou, M. Z. Show-o: One single transformer to unify multimodal understanding and generation. *arXiv preprint arXiv:2408.12528*, 2024.

Xu, P., Jiang, B., Hu, X., Luo, D., He, Q., Zhang, J., Wang, C., Wu, Y., Ling, C., and Wang, B. Unveil inversion and invariance in flow transformer for versatile image editing. In *Proceedings of the Computer Vision and Pattern Recognition Conference*, pp. 28479–28489, 2025.

Yang, K., Shen, B., Li, X., Dai, Y., Luo, Y., Ma, Y., Fang, W., Li, Q., and Wang, Z. Fia-edit: Frequency-interactive attention for efficient and high-fidelity inversion-free text-guided image editing. *arXiv preprint arXiv:2511.12151*, 2025.

Ye, Y., He, X., Li, Z., Lin, B., Yuan, S., Yan, Z., Hou, B., and Yuan, L. Imgedit: A unified image editing dataset and benchmark. *arXiv preprint arXiv:2505.20275*, 2025.

Zhang, L., Rao, A., and Agrawala, M. Adding conditional control to text-to-image diffusion models. In *Proceedings of the IEEE/CVF international conference on computer vision*, pp. 3836–3847, 2023.

Zhao, S., Chen, D., Chen, Y.-C., Bao, J., Hao, S., Yuan, L., and Wong, K.-Y. K. Uni-controlnet: All-in-one control to text-to-image diffusion models. *Advances in Neural Information Processing Systems*, 36:11127–11150, 2023.

## A. SNR-Bench Case Showcase

**SNR-Bench** comprises 80 high-quality image-editing cases. Approximately 50% are sampled from PIE-Bench to ensure continuity with standard benchmarks, and the remaining 50% are collected from the web to introduce richer textures and more complex real-world scenes. We cover four editing operations: *adjust*, *change*, *remove*, and *add*. To minimize ambiguity and improve instruction consistency, all editing instructions for the non-PIE-Bench subset are **manually written, refined, and verified** through human annotation.

### A.1. What we show.

In this section, we provide representative visual examples selected from the 80 cases. Each example includes the source image  $X_{\text{src}}$ , the original/edited prompts (with the edited instruction  $c_{\text{edit}}$ ), and edited outputs  $X_{\text{edit}}$  from different methods. The showcased cases span diverse edit types and difficulty levels, illustrating the challenges in SNR-Bench and complementing our quantitative results on structural fidelity, text-image alignment, and background consistency.

### A.2. Case showcase.

To demonstrate the diversity and complexity of our evaluation set, Figure 9 provides a gallery of representative source images from SNR-Bench. The dataset is designed to cover a broad spectrum of semantic domains and structural types, ensuring a comprehensive assessment of editing capabilities. As shown in the figure, the cases are categorized into distinct groups:

- **Animals & Humans:** Images containing complex biological structures that require fine-grained preservation of identity and texture.
- **Landscapes & Architecture:** Scenes with rich depth information and rigid geometric structures, testing the model’s ability to maintain spatial layout.
- **Patterns & Text (OCR):** Highly structured inputs such as repetitive geometric patterns and legible text. These cases serve as rigorous stress tests for structural fidelity, as even minor trajectory drifts can lead to noticeable distortions or legibility loss.

These diverse categories ensure that SNR-Edit is evaluated across varying levels of difficulty, ranging from organic object manipulation to rigid structural preservation.

## B. Theoretical Analysis of Rectified Noise Distribution

In this section, we provide a theoretical justification for the proposed **Structure-Aware Noise Rectification (SNR)** mechanism. A primary concern when injecting structural priors into the initialization of flow-based models is the potential *distribution shift* (OOD issue). Since pre-trained backbones are optimized under the assumption that the stochastic component is sampled as  $\xi \sim \mathcal{N}(0, I)$ , substantially altering the input scale may lead to artifacts. Throughout this appendix, we use  $v_{\theta}(\cdot, t, c)$  interchangeably with  $v(\cdot, t, c)$  in the main paper.

We show that our **prior preparation** (resize + min–max normalization + broadcasting) constrains the structural prior to a bounded range consistent with the latent noise scale used by the backbone, while preserving relative structural semantics across regions. In addition, we provide a Lipschitz stability bound that justifies the **re-anchored velocity evaluation** in Equation (6) (cf. Section B.3).

### B.1. Structure-Preserving Min–Max Normalization

Let  $\Phi_{\text{map}} \in \mathbb{R}^{H \times W}$  denote the raw single-channel structural map constructed in Phase 1 (cf. Equation (4)). A naive standardization approach (e.g., Z-score normalization) enforces zero mean and unit variance:

$$\hat{\Phi}_{z\text{-score}} = \frac{\Phi_{\text{map}} - \mu_{\Phi}}{\sigma_{\Phi}}. \quad (8)$$

However, such normalization may amplify low-contrast regions or suppress informative inter-region contrasts, weakening the relative structural cues encoded by region-wise intensities. Instead, we adopt a **range-constrained min–max normalization**



Figure 9: **Overview of SNR-Bench Diversity.** We display representative source images from our constructed benchmark, covering six major categories: *Animals*, *Humans*, *Landscapes*, *Architecture*, *Patterns*, and *OCR/Text*. This diversity ensures a robust evaluation of structural consistency across both organic textures and rigid geometric layouts.

consistent with our implementation.

Specifically, we first resize  $\Phi_{\text{map}}$  to the latent resolution, denoted as  $\Phi_{\text{map}}^{\downarrow}$ , and normalize it to the bounded interval  $[-1, 1]$ :

$$\Phi_{\text{norm}} = \left( \frac{\Phi_{\text{map}}^{\downarrow} - \min(\Phi_{\text{map}}^{\downarrow})}{\max(\Phi_{\text{map}}^{\downarrow}) - \min(\Phi_{\text{map}}^{\downarrow}) + \varepsilon} \times 2 - 1 \right), \quad (9)$$

with a zero-map fallback when  $\max(\Phi_{\text{map}}^{\downarrow}) - \min(\Phi_{\text{map}}^{\downarrow})$  is negligible. This affine mapping yields two key properties:

1. **Preservation of Relative Structure:** Min–max normalization is order-preserving and applies an affine transform, thus largely maintaining region-wise intensity ordering and relative contrasts that encode coarse geometry.
2. **Bounded Magnitude:** The structural signal is explicitly bounded as  $\Phi_{\text{norm}}(x) \in [-1, 1]$  for any spatial location  $x$ , preventing uncontrolled magnitude growth.

Finally, we broadcast  $\Phi_{\text{norm}}$  across latent channels to obtain the latent structural prior  $\Phi_{\mathcal{Z}}$  used in Phase 2; this operation changes only tensor shape, not value range. By construction,  $\Phi_{\mathcal{Z}}$  is already at the latent resolution after resizing  $\Phi_{\text{map}}$  and broadcasting.

## B.2. Defense Against Distribution Shift and Rectification Stability

We model the rectified noise  $\tilde{\epsilon}$  as a linear combination of the bounded structural prior  $\Phi_{\mathcal{Z}}$  and the stochastic component  $\xi \sim \mathcal{N}(0, I)$ :

$$\tilde{\epsilon} = \lambda_{\text{struct}} \Phi_{\mathcal{Z}} + \lambda_{\text{stoch}} \xi. \quad (10)$$

We then form the corrected source state  $\tilde{Z}_t^{\text{src}} = (1-t)Z_{\text{src}} + t\tilde{\epsilon}$  and the offset  $\Delta\tilde{Z}_t = \tilde{Z}_t^{\text{src}} - Z_{\text{src}}$ , consistent with Equations (6) and (7).

**Bounded Prior, Controlled Mixing.** By construction,  $\Phi_{\mathcal{Z}}$  is bounded element-wise in  $[-1, 1]$ . Therefore, the structural term has a controlled amplitude determined by  $\lambda_{\text{struct}}$ , while the stochastic term remains Gaussian. This design avoids introducing arbitrarily large perturbations that could push latent features into extreme activation regimes of the pre-trained backbone.

**Energy Consistency.** The min–max normalization establishes a unified and bounded numerical scale for the structural prior, so the mixing coefficients  $\lambda_{\text{stoch}}$  and  $\lambda_{\text{struct}}$  operate on consistent magnitudes. Consequently, the prior is neither overwhelmed by Gaussian noise nor dominates to cause artifacts, promoting stable rectification during ODE integration.

**Practical Robustness.** Although the resulting  $\tilde{\epsilon}$  is not strictly Gaussian due to the additive bounded component, it can be interpreted as a Gaussian perturbation with a bounded, element-wise mean shift induced by  $\Phi_{\mathcal{Z}}$ . This rectification thus acts as a mild, controlled bias on the initialization that empirically avoids severe out-of-distribution behavior while improving structural fidelity.

### B.3. Re-anchored Velocity Evaluation: A Lipschitz Stability Bound

This subsection provides a justification for the **re-anchored velocity evaluation** in Equation (6). We show that, under a standard Lipschitz assumption on the backbone velocity field, re-anchoring yields a controlled vector-field error and thus a bounded trajectory deviation.

**Setup.** Let the ideal source trajectory be  $Z_t^{\text{src}}$ , and define the ideal inversion-free editing dynamics

$$\dot{Z}_t^* = v_{\theta}(Z_t^*, t, c_{\text{tar}}) - v_{\theta}(Z_t^{\text{src}}, t, c_{\text{src}}). \quad (11)$$

In practice, we only have a proxy source trajectory  $\tilde{Z}_t^{\text{src}}$ . Our method uses the *re-anchoring offset*

$$\Delta \tilde{Z}_t = \tilde{Z}_t^{\text{src}} - Z_{\text{src}}, \quad (12)$$

and evaluates the target velocity at a shifted point:

$$\dot{Z}_t = v_{\theta}\left(Z_t + \Delta \tilde{Z}_t, t, c_{\text{tar}}\right) - v_{\theta}\left(\tilde{Z}_t^{\text{src}}, t, c_{\text{src}}\right), \quad (13)$$

which matches Equation (6) in the main paper.

For a fair comparison under the same anchoring coordinate system, we rewrite the ideal target evaluation at the anchored input  $z + (Z_t^{\text{src}} - Z_{\text{src}})$ .

**Assumption (Lipschitz velocity field).** Assume that for each conditioning  $c \in \{c_{\text{tar}}, c_{\text{src}}\}$ , the velocity field is Lipschitz in the latent input:

$$\|v_{\theta}(z_1, t, c) - v_{\theta}(z_2, t, c)\| \leq L_c \|z_1 - z_2\| \quad \forall z_1, z_2, t. \quad (14)$$

**Proxy error.** Define the source-proxy error as

$$\varepsilon_{\text{src}}(t) = \|\tilde{Z}_t^{\text{src}} - Z_t^{\text{src}}\|. \quad (15)$$

**Theorem (Controlled vector-field error of re-anchoring).** Let  $\tilde{f}(z, t) = v_{\theta}(z + \Delta \tilde{Z}_t, t, c_{\text{tar}}) - v_{\theta}(\tilde{Z}_t^{\text{src}}, t, c_{\text{src}})$  be our re-anchored vector field, and let  $f^*(z, t) = v_{\theta}(z + (Z_t^{\text{src}} - Z_{\text{src}}), t, c_{\text{tar}}) - v_{\theta}(Z_t^{\text{src}}, t, c_{\text{src}})$  be the ideal field associated with Equation (11) under the same anchoring reference. Under Equation (14), for any  $z, t$ ,

$$\|\tilde{f}(z, t) - f^*(z, t)\| \leq (L_{\text{tar}} + L_{\text{src}}) \varepsilon_{\text{src}}(t). \quad (16)$$

**Proof.** By triangle inequality and Equation (14),

$$\begin{aligned} \|\tilde{f}(z, t) - f^*(z, t)\| &= \left\| v_{\theta}(z + \Delta \tilde{Z}_t, t, c_{\text{tar}}) - v_{\theta}(z + (Z_t^{\text{src}} - Z_{\text{src}}), t, c_{\text{tar}}) \right. \\ &\quad \left. + v_{\theta}(Z_t^{\text{src}}, t, c_{\text{src}}) - v_{\theta}(\tilde{Z}_t^{\text{src}}, t, c_{\text{src}}) \right\| \\ &\leq L_{\text{tar}} \|\Delta \tilde{Z}_t - (Z_t^{\text{src}} - Z_{\text{src}})\| + L_{\text{src}} \|\tilde{Z}_t^{\text{src}} - Z_t^{\text{src}}\| \\ &= (L_{\text{tar}} + L_{\text{src}}) \varepsilon_{\text{src}}(t), \end{aligned} \quad (17)$$

which proves Equation (16).

**Trajectory deviation bound (ODE stability).** Assume additionally that  $\tilde{f}(\cdot, t)$  is Lipschitz in  $z$  with constant  $L_{\text{tar}}$ , and that  $Z_{t_0} = Z_{t_0}^*$  at the starting time  $t_0$  (e.g.,  $t_0 = t_{\max}$  in Alg. 1). A standard Grönwall argument yields

$$\|Z_t - Z_t^*\| \leq \int_{t_0}^t \exp(L_{\text{tar}}(t-s)) (L_{\text{tar}} + L_{\text{src}}) \varepsilon_{\text{src}}(s) ds. \quad (18)$$

The above bound applies to the continuous-time dynamics for a fixed rectified source proxy (or conditionally on a fixed noise realization); the practical discretization with per-step noise resampling can be viewed as a stochastic Euler approximation.

Therefore, reducing  $\varepsilon_{\text{src}}$  (via SNR rectification and improved source proxying) provably controls the deviation from the ideal editing dynamics.

## C. VLM/Reward-Model Evaluation Setup

To complement pixel-level metrics that may miss global coherence and perceptual artifacts, we conduct model-based evaluation on **SNR-Bench** (80 cases). Note that **SNR-Bench** is the benchmark, while **SNR-Edit** is the proposed method.

### C.1. Evaluators.

We use two evaluators: (1) **ImgEdit Reward** (Ye et al., 2025) (<https://huggingface.co/datasets/syuyy/ImgEdit>), a reward model specialized for image editing evaluation; (2) **Qwen3-VL-32B-Instruct** (Bai et al., 2025) (<https://huggingface.co/Qwen/Qwen3-VL-32B-Instruct>), an open-source VLM used as an evaluator.

### C.2. Unified prompt (BASE\_PROMPT) and I/O.

Both evaluators use the **same** prompt template `BASE_PROMPT` (included below). The inputs include the Original Prompt, the Edited Prompt, the Original Image (first image), and the Edited Image (second image). The evaluator outputs **integer scores** in [0, 5] for three dimensions: (1) Structural Fidelity, (2) Text-Image Alignment, (3) Background Consistency. We directly parse and record these three scores for reporting.

### C.3. Decoding settings and robustness.

To reduce stochasticity and improve reproducibility, we use deterministic decoding for Qwen3-VL-32B-Instruct (e.g., temperature set to 0 with sampling disabled). Outputs that violate the JSON schema or contain scores outside the integer range 0–5 are treated as invalid and automatically re-queried until a parseable output is obtained.

### C.4. BASE\_PROMPT.

```
BASE_PROMPT = (
    "You are an expert image editing evaluation model. You will evaluate the quality of
    an edited image compared to the original image.\n\n"
    "##Input Information:##\n"
    "- Original Prompt: <original_prompt>\n"
    "- Edited Prompt: <edited_prompt>\n"
    "- Original Image: [First image]\n"
    "- Edited Image: [Second image]\n\n"
    "##Evaluation Task:##\n"
    "Evaluate the edited image across the following three dimensions. For each dimension
    , provide a score from 0 to 5:\n"
    "- 0: Completely fails the criterion\n"
    "- 1: Poor quality with major issues\n"
    "- 2: Below average with noticeable problems\n"
    "- 3: Acceptable quality with minor issues\n"
    "- 4: Good quality with very minor flaws\n"
    "- 5: Excellent quality, meets all requirements\n\n"
    "##Evaluation Dimensions:##\n"
    "1. ##Structural Fidelity (structural_fidelity)##: Focus on the consistency of
    entities in the edited image compared to the original. "
    "Evaluate whether the structure, pose, orientation, and spatial relationships of
    objects/subjects remain consistent with the original image. "
```

```

"Unedited entities should maintain their original structure, action, and direction.
Score 5 if entity consistency is perfectly preserved, score 0 if completely
inconsistent.\n\n"
"2. **Text-Image Alignment (text_image_alignment)**: How well does the edited image
match the edited prompt? "
"The edited content should accurately reflect the requested changes described in the
edited prompt. Score 5 for perfect alignment, score 0 for no alignment.\n\n"
"3. **Background Consistency (background_consistency)**: Evaluate the consistency of
all regions EXCEPT the edited subject/object. "
"The background and all unedited parts should remain identical to the original image.
Check for unwanted changes, color shifts, or distortions "
"in areas that should not be modified. Score 5 for perfect consistency of non-edited
regions, score 0 for major inconsistencies.\n\n"
"**Important Guidelines:**\n"
"- Be critical and use the full range of scores (0-5). Avoid clustering all scores
around 3-4.\n"
"- Different images will have different quality levels - some edits are inherently
harder than others.\n"
"- A perfect score (5) should be rare and reserved for truly excellent results.\n"
"- Scores below 2 should be given when there are significant failures.\n"
"- Consider the difficulty of the edit when scoring, but maintain consistent
standards.\n\n"
"**Output Format:**\n"
"Provide your evaluation in the following JSON format:\n"
"```json\n"
"{\n"
"  \"structural_fidelity\": <score>, \n"
"  \"text_image_alignment\": <score>, \n"
"  \"background_consistency\": <score>, \n"
"  \"explanation\": {\n"
"    \"structural_fidelity\": <brief explanation>, \n"
"    \"text_image_alignment\": <brief explanation>, \n"
"    \"background_consistency\": <brief explanation>\n"
"  }\n"
"}\n"
"```\n\n"
"Now evaluate the images and provide your scores in the JSON format above."
)

```

## D. User Study Details

### D.1. Goal

To validate whether automated metrics reflect human perception, we conduct a user study on **SNR-Bench**. We evaluate edited images from three aspects: **Structural Fidelity**, **Text-Image Alignment**, and **Background Consistency**.

### D.2. Cases and Randomization

The study includes **80 editing cases** from SNR-Bench. Each case consists of a source image  $X_{\text{src}}$ , an editing instruction  $c_{\text{edit}}$ , and edited outputs produced by different methods  $\{X_{\text{edit}}^{(m)}\}_{m=1}^M$ . All cases are **shuffled randomly** before being presented to participants.

### D.3. Rating Dimensions and Scale (Integer 0–5)

Participants assign integer scores in  $\{0, 1, 2, 3, 4, 5\}$  for each edited image:

- **Structural Fidelity (0–5):** Consistency of entities with the original image. Unedited parts should preserve their original structure, pose, and orientation.
- **Text-Image Alignment (0–5):** How well the edited image matches the editing prompt.

- **Background Consistency (0–5):** Consistency of all unedited regions. The background and all non-target areas should remain consistent with the source image.

We instruct participants that higher scores indicate better performance on the specified dimension, rather than overall aesthetic preference.

#### D.4. Procedure and Workload

Each task page shows the source image  $X_{\text{src}}$ , the editing instruction  $c_{\text{edit}}$ , and one edited output  $X_{\text{edit}}^{(m)}$ . Participants provide three integer ratings (0–5) for the three dimensions above. The number of cases labeled by each participant is **randomly assigned and/or self-paced**, with a minimum requirement of **20 cases per participant**, denoted by  $T_p \geq 20$ . Therefore, participants may complete different numbers of cases.

#### D.5. Blinding and Order Randomization

To reduce potential biases:

- **Blinding:** Method identities are hidden; participants only see anonymized outputs without method names.
- **Randomized order:** The order of cases is randomized per participant. The presentation order of methods within the same case is also randomized to mitigate position bias and learning effects.

#### D.6. Quality Control

We apply basic quality-control rules to filter invalid submissions (e.g., missing ratings or clearly careless responses). Optionally, a small number of control items (e.g., no-edit outputs or outputs that clearly contradict the prompt) can be included to verify attention consistency. Submissions flagged as invalid are excluded from analysis.

#### D.7. Aggregation and Statistics

Let  $s_{p,i,m}^{(d)} \in \{0, \dots, 5\}$  be participant  $p$ 's rating on the  $i$ -th labeled case for method  $m$  under dimension  $d \in \{\text{Struct, Text, BG}\}$ . Since participants may complete different numbers of cases ( $T_p$  varies), we aggregate scores by **first averaging within each participant** and then averaging across participants, preventing participants with larger workloads from dominating the overall mean:

$$\bar{s}_{p,m}^{(d)} = \frac{1}{T_p} \sum_{i=1}^{T_p} s_{p,i,m}^{(d)}, \quad \bar{s}_m^{(d)} = \frac{1}{|\mathcal{P}|} \sum_{p \in \mathcal{P}} \bar{s}_{p,m}^{(d)},$$

where  $\mathcal{P}$  denotes the set of valid participants. We report  $\bar{s}_m^{(d)}$  in the main paper (Table 2).